Mesocellular Foam Carbons: Aggregates of Hollow Carbon Spheres with Open and Closed Wall Structures

Yukito Oda,[†] Katsuya Fukuyama,[‡] Keiko Nishikawa,[§] Seitaro Namba,[||] Hideaki Yoshitake,[⊥] and Takashi Tatsumi*[,†]

Graduate School of Engineering, Yokohama National University, Tokiwadai, Hodogaya-ku, Yokohama 240-8501, Japan, Department of Chemistry, Keio University, Hiyoshi, Kohoku-ku, Yokohama 223-8521, Japan, Graduate School of Science and Technology, Chiba University, Yayoicho, Inage-ku, Chiba 263-8522, Japan, Department of Materials, Teikyo University of Science & Technology, Uenohara-machi, Kitatsuru-gun, Yamanashi 409-0193, Japan, and Graduate School of Environment and Information Sciences, Yokohama National University, Tokiwadai, Hodogaya-ku, Yokohama 240-8501, Japan

Received April 5, 2004. Revised Manuscript Received July 6, 2004

A mesostructured hollow sphere form of carbon can be synthesized by using mesocellular foam (MCF) silica as template. A carbon structure composed of spherical hollows with closed walls and with mesopores of around 4 nm in diameter was prepared by the two-step impregnation of sucrose and successive carbonization under flowing argon at 900 °C. A temperature-programmed oxidation experiment revealed that the mesoporous carbon released argon atoms when heated above 600 °C, when oxidation of the carbon walls occurred. This result provides evidence for the presence of a large void volume inside the carbon spheres and implies that the pore size of 4 nm is due to the interspheric space. A single-step impregnation of sucrose resulted in the formation of open-walled mesospheres with pores of 4, 18, and 24 nm. The two larger pore sizes are attributed to the diameters of the window and of the cell as in MCF−silica. Platinum was loaded on these mesoporous carbons. The metal was highly dispersed (∼0.4 nm by EXAFS) on the enclosed mesospheric carbon, while the material that grew in the pores of the open mesospheres consisted of particles that were around 15 nm diameter, as estimated by the Scherrer equation.

Introduction

Mesoporous carbons synthesized using ordered mesoporous silica as a template[1−17] have received great attention as the most successful example of an inverse replication synthesis process. Ordered mesoporous carbon with cubic and hexagonal symmetries can be obtained by using the mesoporous silicas known as MCM-48, SBA-1, and SBA-15. Even when the same template is used, ordered mesoporous carbons consisting of interconnected rods or interconnected tubes can be achieved by simply using different sources[9] and/or quantities[6,16] of carbon. This demonstrates that the nanostructures of mesoporous carbon materials can be varied by carefully tuning the synthesis conditions. The physicochemical properties of these carbons, such as high specific surface area and large pore volume, together with their ordered mesostructure, make them promising candidates for a variety of applications, including catalysis, adsorption, chromatography, photonic devices, and electrochemistry. The recently developed capability for partial templating of the carbon pitch

* To whom correspondence should be addressed. E-mail: ttatsumi@ynu.ac.jp.
[†] Graduate School of Engineering, Yokohama National University.
[‡] Department of Chemistry, Keio University.
[§] Graduate School of Science and Technology, Chiba University.
[||] Department of Materials, Teikyo University of Science & Technology.
[⊥] Graduate School of Environment and Information Sciences, Yokohama National University.

(1) Ryoo, R.; Joo, S. H.; Jun, S. *J. Phys. Chem. B* **1999**, *103*, 7743.
(2) Kruk, M.; Jaroniec, M.; Ryoo R. *J. Phys. Chem. B* **2000**, *104*, 7960.
(3) Ohkubo, T.; Miyazaki, J.; Kaneko, K.; Ryoo R.; Seaton, N. A. *J. Phys. Chem. B* **2002**, *106*, 6523
(4) Jun, S.; Joo, S. H.; Ryoo, R.; Kruk, M.; Jaroniec M.; Liu, Z.; Ohsuna, T.; Terasaki O. *J. Am. Chem. Soc.* **2000**, *122*, 10712.
(5) Lee, J. S.; Joo, S. H.; Ryoo, R. *J. Am. Chem. Soc.* **2002**, *124*, 1156.
(6) Joo, S. H.; Ryoo, R.; Kruk, M.; Jaroniec, M. *J. Phys. Chem. B* **2002**, *106*, 4640.
(7) Kruk, M.; Jaroniec, M.; Joo, S. H.; Ryoo R. *J. Phys. Chem. B* **2003**, *107*, 2205.
(8) Kaneda, M.; Tsubakiyama, T.; Carlesson, A.; Sakamoto, Y.; Ohnuma, T.; Terasaki, O.; Joo, S. H.; Ryoo, R. *J. Phys. Chem. B* **2002**, *106*, 1256.
(9) Joo, S. H.; Choi, S. J.; Oh, I.; Kwak, J.; Liu, Z.; Terasaki, O.; Ryoo, R. *Nature* **2001**, *412*, 169.
(10) Kruk, M.; Jaroniec, M.; Kim, T. W.; Ryoo, R. *Chem. Mater.* **2003**, *15*, 2815.
(11) Darmstadt, H.; Roy, C.; Kaliaguine, S.; Kim, T. W.; Ryoo, R. *Chem. Mater.* **2003**, *15*, 3300.
(12) Joo, S. H.; Shinae, J.; Ryoo, R. *Microporous Mesoporous Mater.* **2001**, *44*−*45*, 153.
(13) Solovyov, L. A.; Zaikowskii, V. I.; Shmakov, A. N.; Belousov, O. V.; Ryoo, R. *J. Phys. Chem. B* **2002**, *106*, 12198.
(14) Kim, T. W.; Park, I. S.; Ryoo, R. *Angew. Chem., Int. Ed.* **2003**, *42*, 4375.
(15) Lu, A.; Kiefer, A.; Schmit, W.; Schüth, F. *Chem. Mater.* **2004**, *16*, 100.
(16) Lu, A.; Schmidt, W. Spliethoff, B.; Schüth, F. *Adv. Mater.* **2003**, *15*, 1602.
(17) Lee, J.; Yoon, S.; Oh, S. M.; Shin, S.; Hyeon, T. *Adv. Mater.* **2000**, *12*, 359.

10.1021/cm0494296 CCC: $27.50
Published on Web 09/11/2004

with using ordered mesoporous silicas has enhanced the thermal stability and (probably) the electrical conductivity of the material.[18,19] While an improvement in stability and conductivity is critically important for industrial applications, the pore diameter (typically in the range of 2−10 nm in most of the examples reported in the literature) would prevent mesoporous carbon from gaining wide usage. Larger pores will be necessary for some applications such as Pt-supported catalysts for fuel cell electrodes, where the metal particles in the pores need to make contact with with residual chains of the polymer membrane without interfering with the diffusion of fuel and oxidant gases.

Transmission microscope images of mesocellular siliceous foam (MCF-silica) have revealed a wide range of internal pore sizes (24−42 nm) and window sizes (9−19 nm), according to the amount of the additives 1,3,5-trimethylbenzene and NH_4F that are used in the surfactant solution.[20,21] This type of silica has shown extremely large pore volumes, with a maximum of $V_P = 2.4$ cm^3 g^{-1}, which is consistent with the foam structure. Lee et al. synthesized a bimodal mesoporous carbon by using the micropores inside the walls of MCF−silica−alumina.[22] According to their model, templating did not result in inverse replication. In this study, we demonstrate the synthesis of mesoporous carbon in a foam replica by templating with MCF-silica. We show that the carbon foam is an ordered aggregation of hollow carbon spheres and that we can control whether the spheres are open or closed by altering the synthesis conditions.

Most of such carbons have been prepared by the polymerization of organic compound and subsequent carbonization under inert conditions, which are followed by dissolution of silica template with hydrogen fluoride or sodium hydroxide. This procedure can provoke the change in chemical properties of the carbon surface that is contact with silica before removal by dissolution. In the carbon with larger mesopores, the difference will more clearly appear after the chemical modification of the surface such as loading of metal particles. We also show the selective platinum loading in reflecting the difference of the carbon surfaces.

Experimental Section

Material Preparation. Mesocellular foam silica (MCF−silica) was prepared by the method described in ref 20. In a typical procedure, 2 g of the triblock copolymer Pluronic P123 (BASF) was dissolved in 75 mL of a 1.6 M HCl aqueous solution at room temperature followed by the dissolution of a known amount (1, 2, 3, or 5 g) of 1,3,5-trimethylbenzene (TMB, Tokyo Kasei Kogyo Co., Ltd., reagent grade). The mixture was stirred at 35−40 °C for 1 h before the addition of 4.4 g of tetraethyl orthosilicate (TEOS, Tokyo Kasei Kogyo Co., Ltd., reagent grade). The solution was stirred for 20 h and aged at 100 °C for 24 h under static conditions. The white precipitate that formed after standing at room temperature was filtered, dried, and calcined at 500 °C for 8 h. The various silica structures that were obtained are denoted as S1, S2, S3, and S4, respectively.

These MCF−silicas were impregnated with an aqueous solution of sucrose (Junsei Chemical co.) and sulfuric acid. The typical molar composition of the solution was $C_{12}H_{22}O_{12}$:H_2SO_4:H_2O = 2.88:0.32:11.5. The mixture was heated at 100 °C for 6 h and subsequently at 160 °C for 1 h. This impregnation-drying process was then repeated, though the second loading with sucrose was lower than that in the first step in order to avoid the formation of carbon outside the pores in the silica. The carbonization was completed by heating at 900 °C for 6 h under flowing argon. The silica was removed from the silica−carbon composite by treating it with hydrofluoric acid, washing with ethanol, and then drying in air. The MCF carbons derived from the various S*n* MCF-silica templates were denoted as C*n* (where n = 1, 2, 3, and 4). The MCF carbon prepared by a single impregnation (i.e., without repetition of sucrose loading) of S3 was named C3*.

Platinum-loaded MCF carbons were then prepared using the following incipient wetness method. Samples of MCF carbon were soaked with a solution of $[Pt(NH_3)_4](NO_3)_2$ (Alfa Aesar) dissolved in formic acid, which was then calcined at 200 °C for 2 h and reduced in a hydrogen flow at 450 °C for 3 h. The platinum loading was 2 wt %.

Characterization. The nitrogen adsorption−desorption isotherms were recorded using a BELSORP 28SA (BEL Japan Inc.) after the samples had been evacuated at 473 K for 2 h. The pore size distributions were calculated by the D−H method.[23] The BET surface area was obtained over a relative pressure (P/P_0) range of 0.05−0.18. Small-angle X-ray scattering (SAXS) experiments were performed in a transmission mode on a handmade diffractometer using an asymmetric channel-cut monochromator and Cu Kα_1 radiation (λ = 0.15406 nm).[24]The powder particles were observed by transmission electron microscopy (TEM) using a JEOL JEM-2000EX at 100- or 200-kV acceleration voltage. Temperature-programmed oxidation (TPO) was performed with a TPD-39 (BEL Japan inc.) at a heating rate of 5 °C/min. The gas-phase products were analyzed using a quadrupole mass spectrometer. Pt L_3 edge EXAFS spectra were measured in the Beamline 10 B at the Photon Factory, High Energy Accelerator Research Organization, Tsukuba, Japan (Proposal #2004G125), where a conventional transmission mode with detection using gas ion chambers was employed. Analysis of the EXAFS data[25] has been described in the Supporting Information.

Results and Discussion

MCF−Silica Structure. The nitrogen adsorption/desorption isotherms are type IV and show steeply sloped isotherms and large hystereses at high relative pressures, as shown in Figure 1. Although the curves for S1 did not show a steep step, they are still categorized into type IV. This feature is typical of mesoporous materials that exhibit capillary condensation/evaporation and have large pore sizes with narrow size distributions. The increase in the steepness and the shift of the position with increasing concentration of TMB agrees with the graphs in ref 20. A sharp peak from the desorption data and a broad peak from the adsorption data were found in the case of the pore size distributions shown in the inset of Figure 1. The gradually increasing pore size from the desorption branch has been attributed to the window of the silica

(18) Vix-Guterl, C.; Saadallah, S.; Vidal, L.; Mohamad, R.; Parmentier, J.; Patarin, J. *J. Mater. Chem.* **2003**, *13*, 2535.
(19) Li, Z.; Jaroniec, M. *J. Phys. Chem. B* **2004**, *108*, 824.
(20) Schimidt-Winkel, P.; Lukens, W. W., Jr.; Ying, P.; Margolese, D. I.; Lettow, J. S.; Ying, J. Y.; Stucky, G. D. *Chem. Mater.* **2000**, *12*, 686.
(21) Lettow, J. S.; Han, Y. J.; Schmidt-Winkel, P.; Yang, P.; Zhao, D.; Stucky, G. D.; Ying, J. Y. *Langmuir*, **2000**, *16*, 8291.
(22) (a) Lee, J.; Sohn, K.; Hyeon, T. *J. Am. Chem. Soc.* **2001**, *123*, 5146. (b) Kim, M.; Yoon, S. B.; Sohn, K.; Kim, J. Y.; Shin, C. H.; Hyeon, T.; Yu, J. S. *Microporous Mesoporous Mater.* **2003**, *63*, 1.
(23) Dollimore, D.; Heal, G. R. *J. Colloid. Interface Sci.* **1970**, *33*, 508.
(24) Kasahara, Y.; Nishikawa, K. *Jpn. J. Appl. Phys.* **2000**, *39*, 343.
(25) Yoshitake, H.; Yokoi, T.; Tatsumi, T. *Chem. Mater.* **2003**, *15*, 1713.

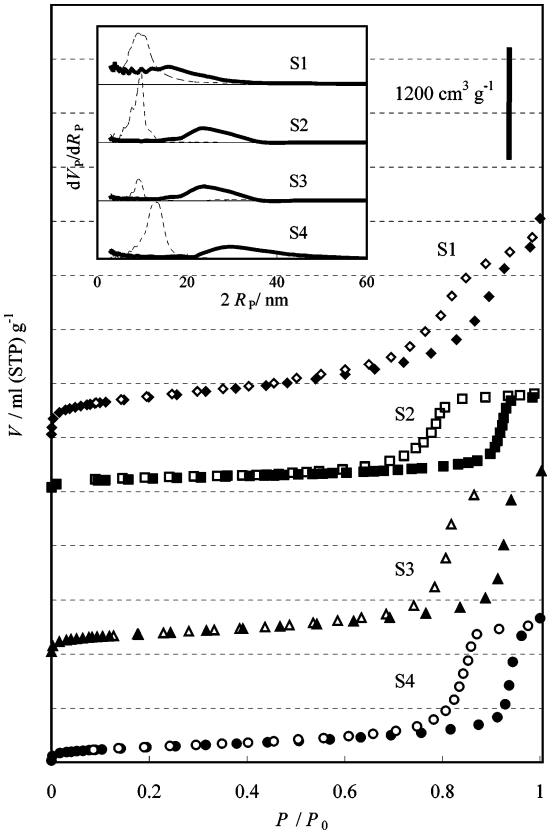

Figure 1. Nitrogen adsorption isotherms and corresponding pore size distributions for MCF−silicas, which were prepared in the ratio TMB/Pluronic P123 = 0.5 (S1), 1.0 (S2), 1.5 (S3), and 2.5 (S4). The solid (blank) dots and the bold (fine) lines are data due to the adsorption (desorption) branch.

Table 1. Mesostructural Characteristics of MCF−Silica

silica	TMB/P123 (w/w)	$2R_P$(ads) nm	$2R_P$ (des) nm	S_{BET} m^2 g^{-1}	V_P cm^3 g^{-1}
S1	0.5	16	9.8	619	3.3
S2	1.0	24	9.8	477	2.3
S3	1.5	24	10	769	3.0
S4	2.5	30	14	569	2.3

cell, while the shifting peak from the adsorption branch has been assigned to the size of the cell.[20,21] The structural parameters deduced from these plots are summarized in Table 1. The large pore volume and size are in agreement with the original report on the synthesis of MCF−silica, though the pore size is slightly different, probably due to the different calculation methods that were used. The BET surface area and the pore volume are complicated and are not in agreement with the previous report. We performed the synthesis of the MCF−silica while varying the rotation of the stirrer. This is a potentially important parameter because the formation of foams will depend considerably on the stirring conditions. The surface area and the pore volumes of the resulting silica samples were, in fact, quite sensitive to the rate of stirring. Nevertheless, the pore sizes did not differ significantly when the speed of rotation was changed in the range between 100 and 600 rpm. These results imply that the loss of surface area and of pore volume is mainly caused by partial failures in the formation of the foam, thereby generating carbon particles without mesostructural characteristics. Since MCF−silica S3 shows large values for S_{BET} and V_p and

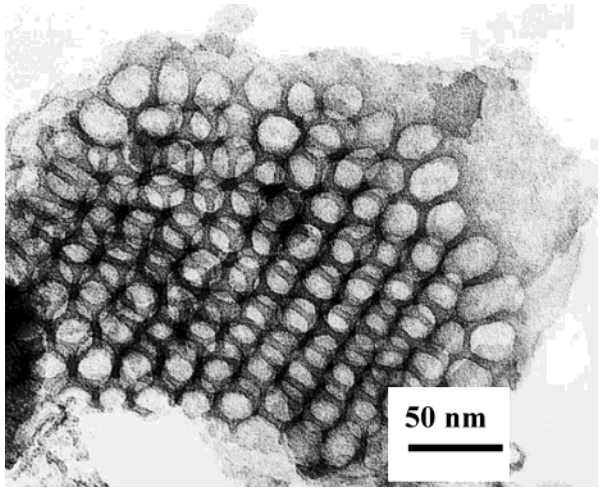

Figure 2. TEM photograph of MCF−silica S3.

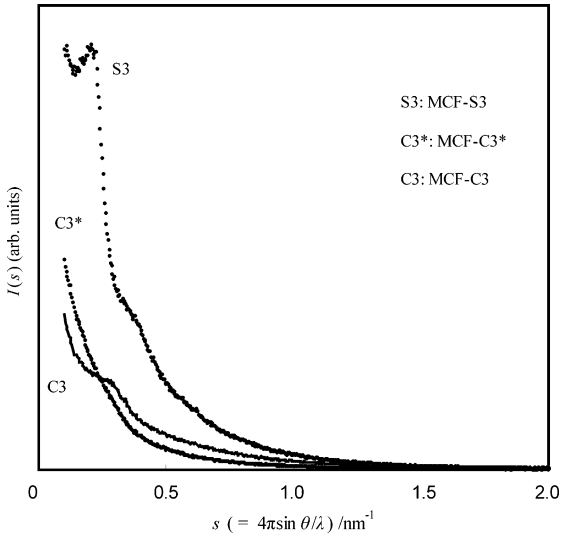

Figure 3. SAXS pattern of MCF−silica S3 and corresponding MCF carbons synthesized using S3 as a template.

is considered to have a uniform structure, it was used as a template for the synthesis of the two kinds of MCF carbon described below.

Figure 2 shows a TEM photograph of the MCF−silica. The cells, which are 20 nm in diameter, are found to exist in a hexagonal array, unlike previously reported examples of MCF.[20] The second layer in the cell array is also hexagonally packed but not commensurate with the first layer. The average distance between the circles is 25 nm. TEM images with the same characteristics were obtained for the other MCF−silicas, where the cell size increased with increasing concentration of TMB.

The SAXS patterns for MCF−silica S3 are plotted in Figure 3, together with those of the mesoporous carbons that were synthesized using it as a template. Three peaks can be found where s = 0.22, 0.33, and 0.40 nm^{-1}, where the scattering parameter s is defined by 4π sin θ/λ with a scattering angle 2θ and wavelength of X-ray λ. The d-spacings were calculated to be 28.6, 19.0, and 15.7 nm, respectively. When monodispersed spheres with a diameter of 28 nm was assumed, the s will become 0.22, 0.33, and 0.44 nm^{-1}. [20] This is in good agreement with the peak positions observed in the SAXS profile and the estimation by the TEM photograph in Figure 2 (25 nm). When the first peak is

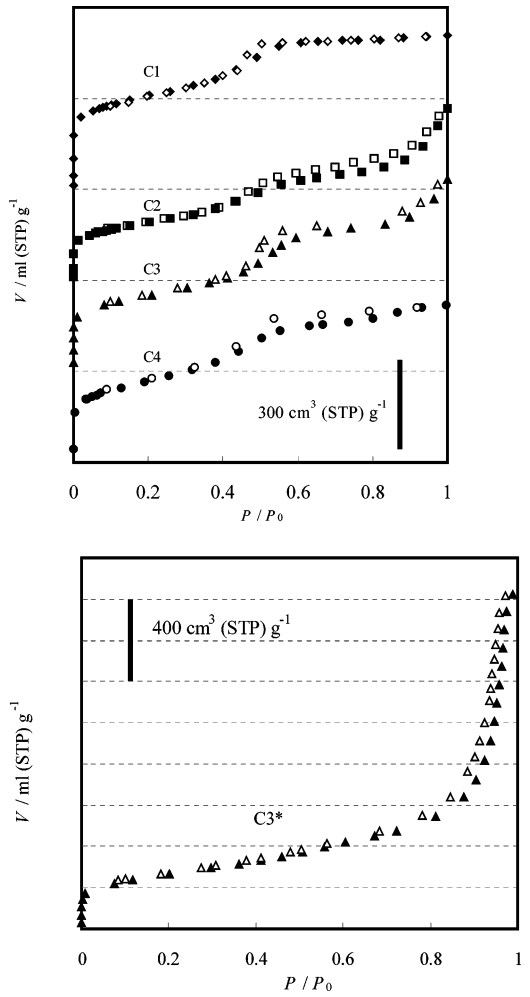

Figure 4. Nitrogen adsorption isotherms of MCF carbons C1, C2, C3, and C4, which were prepared by templating with S1, S2, S3, and S4 silicas, respectively. The template for C3* was MCF−silica S3, for which the sucrose loading was not repeated. The solid and blank dots present the adsorption and desorption of nitrogen, respectively.

attributed to the Bragg reflection of a hexagonal array of spheres, $d_{100} = 28.6$ nm will give a sphere spacing of 33 nm, which is larger than the average distance of neighboring circles in the TEM estimation.

MCF Carbon Structure. Figure 4 shows the nitrogen adsorption isotherms of MCF carbons corresponding to the silicas in Figure 1. Rises in the adsorptions of carbons C1, C2, C3, and C4 appeared at ca. $P/P_0 = 0.5$ (cf. $P/P_0 = 0.7-0.9$ for MCF−silicas) but the step was not as high as those observed for the MCF−silicas in Figure 1. The total amount of adsorption was also significantly reduced. These considerable differences in adsorption features imply that templating with MCF−silica did not result in inverse replication, but in the formation of a different porous structure. The topological difference between the template silica and a resulting carbon has been often pointed out since the reports on CMK-1.[1,2] On the other hand, C3* carbon, which was prepared without the second impregnation with the sucrose solution, showed behavior similar to that of S3 silica in terms of its adsorption step and total amount of nitrogen that it could adsorb. Although the density of the framework of these materials was unknown, it was concluded that the second impregnation process causes a significant structural change from the replica. No large hysteresis was observed, even in the rising region for the C3* carbon, suggesting that the window is enlarged to approach the cell diameter.

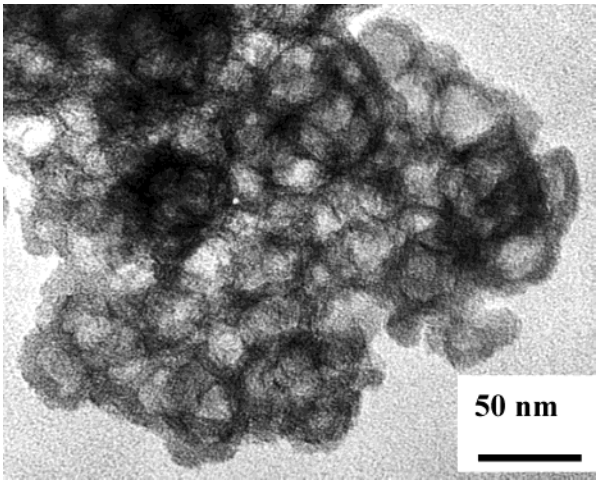

Figure 5. TEM photograph of MCF carbon C3.

A TEM photograph of MCF carbon C3 is shown in Figure 5. The cell array that is hardly ordered, probably due to the lack of formation of the hexagonal plane as can be observed in the image of MCF-S3 (Figure 2). This is consistent with the more diffuse Bragg reflections of MCF-C3 than MCF-S3 in Figure 3. The inner diameter of the cells is ca. 22 nm. The outer diameter, ca. 31 nm, is larger than the diameter of the circle observed in Figure 2, which is 20 nm. This disagreement concurs with the assignment of the open circles in Figure 2 to the image of the window of the MCF−silica. The other possible explanation is a swelling of the carbon during the removal of the silica. The other mesoporous carbons exhibited similar TEM images to Figure 5, though the size of the spheres changed according to the template cell diameter.

The topologically similar images of the MCF−silica and the carbon are apparently contradictory to the different nitrogen adsorption results. The pore size distributions of the mesoporous carbons are shown in Figure 6. Sharp peak peaks were observed at 3.8 ± 0.3 nm in both the adsorption and the desorption branches of carbons C1, C2, C3, and C4. No other features were found in these carbons. In contrast, a peak was observed at 24 nm in the adsorption branch and at 18 nm in the desorption branch in addition to those at 4.5 nm in the distributions for C3*. The difference between 24 and 18 nm is due to a small hysteresis found around $P/P_0 = 0.9$ in the adsorption/desorption isotherms. We attribute the peaks at 18 and 24 nm to the cell diameter and the window size of the MCF carbon, respectively, by analogy with the mesoporous structure of the MCF−silica. The pore sizes, the BET surface area, and the pore volume were calculated using the isotherms and the results are listed in Table 2. The BET surface area is larger than that of the silica template, due to the low density of the carbon framework. Nevertheless, the pore volumes of C1, C2, C3, and C4, all of which were prepared with sufficient supply of sucrose, are much lower than the corresponding templates, implying that the volumes of the mesopores are significantly reduced in the inversely replicating process. On the other hand, C3*, which was

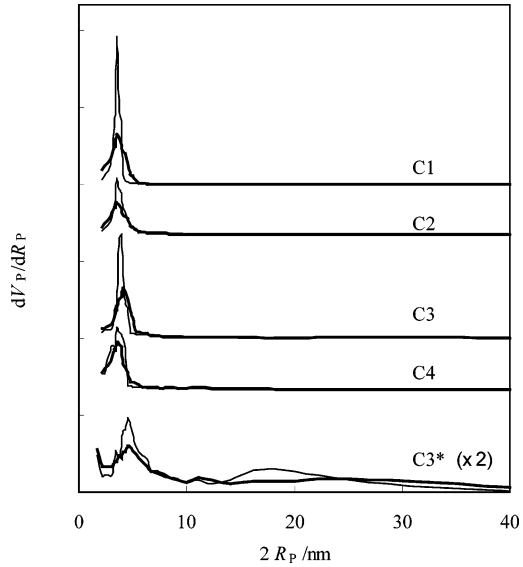

Figure 6. Pore size distributions for MCF carbons C1, C2, C3, and C4, which were prepared by templating with S1, S2, S3, and S4 silicas, respectively. The template for C3* is MCF−silica S3 for which the sucrose loading was not repeated. The bold and fine lines present the adsorption and desorption of nitrogen, respectively.

Table 2. Mesostructural Characteristics of MCF−Carbon

carbon	$2R_P$(ads) nm	$2R_P$ (des) nm	S_{BET} $m^2\ g^{-1}$	V_P $cm^3\ g^{-1}$
C1	3.6	3.6	991	0.56
C2	3.6	3.6	641	0.73
C3	3.7	4.1	817	0.73
C4	3.6	3.6	897	0.66
C3*	4.3, 24	4.5, 18	950	1.8

prepared by a single impregnation step, exhibited a pore volume 2.5 times larger than C3, together with a larger surface area. This result reveals the generation of another kind of mesopore by reducing the amount of carbon in the pores of the MCF−silica. The most likely mesostructure of the C3* carbon is therefore an aggregate of hollow spherical carbons with open walls, which is similar to the structure of the MCF−silica. On the other hand, the pore size of 4 nm that is common among all of the carbon samples cannot directly correspond to the pores of the MCF−silica. Since C1, C2, C3, and C4 did not show pores in the 20 nm range, they are likely to be the aggregates of closed hollow spheres. Considering that this pore size occurs independently of the silica cell, it can be attributed to the openings among the carbon spheres that are formed after the dissolution of the silica. This assignment of the 4 nm pore size to the interparticle pore space is rationalized by the size of the silica walls (3−4 nm) which are imaged in Figure 2. The silica walls can create pores in the MCF carbon after the removal of the silica from the silica−carbon composite.

When we synthesized MCF PAN (polyacrylonitrile) carbon using the same template, peaks were observed at 3.2 and 37 nm in the pore size distributions from the adsorption branch. The former pores are considered to be similar interparticular pores. Hyeon et al. has reported a phenol-resin-based MCF carbon in which they found pores of 3.5 and 27 nm from the adsorption branch and of 3.5 and 14 nm from the desorption

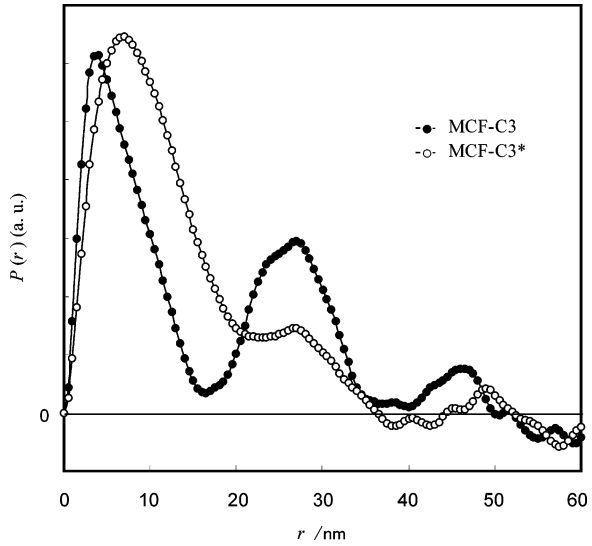

Figure 7. Pair distance distribution functions, $P(r) = (1/(2\pi^2)) \int_0^\infty I(s)sr \sin(sr)\, ds$, of MCF carbons C3 and C3*.

branch.[22a] This pore pattern agrees with that of MCF carbon C3* (4.3, 18, and 24 nm).

The SAXS pattern for MCF carbon C3 in Figure 3 is not as well-resolved as that for the template MCF−silica S3. Only one peak is found at $s = 0.298$ Å^{-1} and this is a shoulder that corresponds to a d spacing of 21 nm. By exclusion of the overlapping images of the cells, the average distance of two neighboring circles could be calculated from the TEM photograph (Figure 5). The measured value of 23 nm agreed quite well with the d spacing from the diffraction pattern. This value was attributed to the distance between the cell centers. The MCF carbon C3* showed a smaller peak at the same position, implying a lowering of the interference of the X-rays. This is consistent with the open-walled structure with the same mode of agglomeration as the closed spheres of C3 carbon. The enlargement of the d spacing from the template MCF−silica suggests a swelling of the lattice structure during the inverse replicating process or the dissolution of the silica.

The pair distance distribution functions (PDDF) obtained from the SAXS patterns of the MCF carbons are plotted in Figure 7. [26] The first peak at 3.5 nm in the PDDF of MCF carbon C3 is the correlation of density arising from the interparticle pore space. The next peak, which rises before $P(r)$ becomes zero, implies that the distorted spherical matter does not adhere to the adjacent points but rather to adjacent faces. Thus, the peak at 23 nm is reasonably attributed to the distance between the sphere centers. The distance is smaller than that between the centers in MCF-S3 (28.6 nm by SAXS), suggesting shrinkage of the lattice during the carbonization and silica dissolution. The peak at 28 nm can be explained as the dimension of the sum of an interparticle pore space and a hollow sphere. In the PDDF of MCF carbon C3*, the first peak shifted to 6.5 nm and the oscillation is not as clearly ordered as that of carbon C3. This can be explained by the carbon wall being thinner than C3 and a part of it has broken to

(26) Glatter; O., Kratky, O. Eds. *Small-Angle X-ray Scattering*; Academic Press: New York, 1982; p 130.

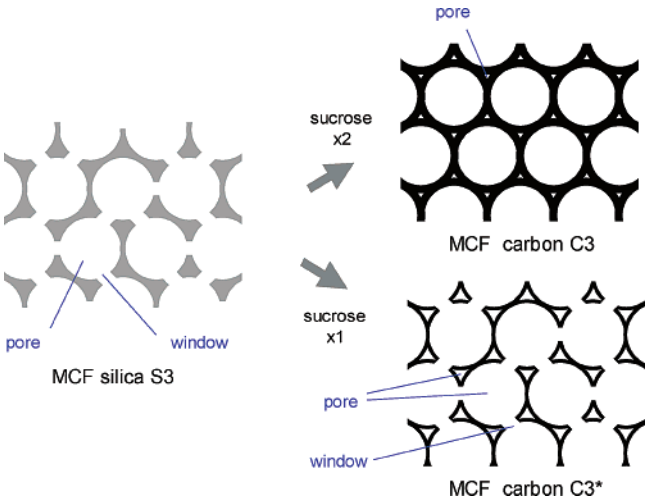

Figure 8. Schematic model of MCF carbon formations.

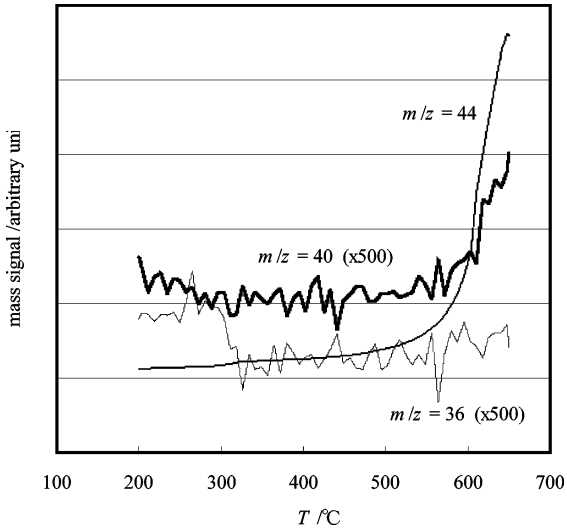

Figure 9. Temperature-programmed oxidation profile of MCF carbon C3. Mass numbers 36, 40, and 44 are plotted. The temperature was raised at a rate of 5 °C/min.

connect the inside of the cells. A detailed analysis of the PDDF is underway.

The pore formation of the MCF carbons is schematically presented in Figure 8. The wall of MCF−silica is inversely replicated into the pore (around 4 nm) of the MCF carbons. The single load of sucrose leads to the formation of open wall MCF carbon C3* while the repetition of loading closes the wall (MCF carbon C3). In other words, the dehydrated sucrose−template composite prepared by a single sucrose impregnation is transformed into an open cell foam after carbonization at 900 °C, while the second sucrose impregnation of this composite results in formation of closed cell foams after the same carbonization. As a result, the inside of the cells is accessible from the outside of the particle in MCF C3* while it becomes voids in MCF C3.

The contribution of the rise in the region where $P/P_0 < 0.2$ to the total nitrogen adsorption of the MCF−silica (Figure 1) is smaller than the other mesoporous silicas such as SBA-15, implying that the development of micropores is not significant in the framework structure. Thus, the mechanism for connection by thin rods that is proposed in the structure of CMK-3 is not likely in MCF carbons because their structure is replicated with that of MCF−silica.

The synthesis of an ordered mesoporous carbon with a large pore size has recently been an intriguing issue. Templates of organic colloids[27,28] and of polystyrene particles[29] have realized large porous carbons. Nevertheless, a hard template for tunable and large mesopores is needed for the inverse replicating method because this technique could take an advantage in preparing ordered mesoporous carbons with various pore sizes.

Characteristics of Mesopores of MCF Carbons. When the hollow spheres prepared under an argon atmosphere are completely closed, Ar atoms will be confined within the spheres. To confirm the existence of argon within the carbon, we performed temperature-programmed oxidation of MCF carbon C3 under flowing oxygen while we analyzed the gas-phase products. The results for mass numbers 36, 40, and 44 (for which the major species are C_3^+, Ar^+, and CO_2^+, respectively) are shown in Figure 9. The increase in the intensity of $m/z = 44$ around 600 °C implies that the oxidation of carbon had started. At the same temperature, the signal for $m/z = 40$ began to increase. This coincidence strongly suggests that the breakdown of the framework wall due to oxidation (which starts around 600 °C) causes the leakage of argon encapsulated in the mesoporous carbon. This plot provides evidence for the presence of isolated voids, which agrees with the closed-hollow sphere model. We monitored $m/z = 38$, which showed no such increase, as did $m/z = 36$. The C3* carbon did not show any evidence for the release of Ar upon oxidation, which strongly suggested that the Ar was present inside the closed spherical cells and not merely in the carbon walls of C3.

TEM images of platinum-loaded MCF carbon C3 and C3* are shown in Figure 10. Finely dispersed Pt particles are observed on carbon C3, while the particles are agglomerated on carbon C3*, despite using the same method and the same amount of loading. The particle size of the Pt/MCF carbon C3* estimated by the Scherrer equation is about 15 nm. Since the width of the diffraction peaks of the Pt on carbon C3 is too large to apply the Scherrer equation, we measured the Pt L_3 EXAFS spectrum. Analysis of the spectrum revealed that the coordination number of the first Pt shell was 7.1 ± 0.3, with a distance of 2.768 ± 0.002 Å and a Debye−Waller factor of 0.070 ± 0.002 Å. The particle size was estimated to be 0.4 nm from the coordination number, assuming that the particles were spherical.[30]

In addition to the large size, the images of all the platinum particles in carbon C3* are found in light shades, which are evidently due to MCF carbon. This characteristic implies that the metal particles are occluded into the carbon. The rims of the carbon in the silhouette are about 8 nm wide, which is comparable to the wall thickness in Figure 5, and can be attributed to the walls of the MCF carbon C3*. Although the existence of fine Pt particles on the outer surface of the open hollow spheres is not certain, the concentration of Pt-

(27) Lukens, W. W.; Stucky, G. D. *Chem. Mater.* **2002**, *14*, 1665.
(28) Li, Z.; Jaroniec, M. *Chem. Mater.* **2003**, *15*, 1327.
(29) Bauman, T. F.; Satcher, J. H., Jr. *Chem. Mater.* **2003**, *15*, 3745.
(30) Greegor, R. B.; Lytle, F. W. *J. Catal.* **1980**, *63*, 476.

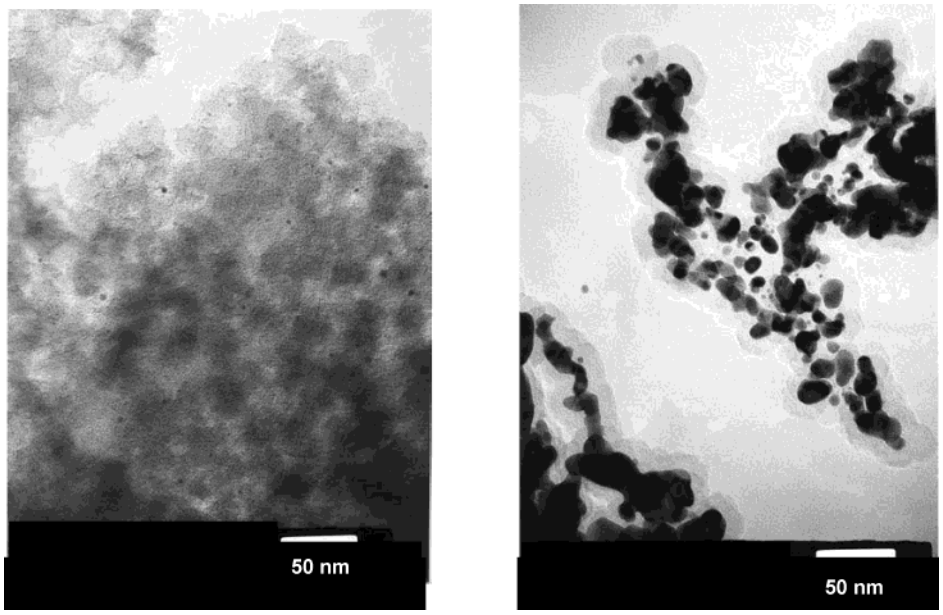

Figure 10. TEM photographs of platinum-loaded MCF carbons C3 (left) and C3* (right). The carbons were impregnated with a formic acid solution of $[Pt(NH_3)_2](NO_2)_2$. The metal loading was 2 wt %.

$(NH_3)_4^+$ and the growth of Pt particles inside of the carbon cell are unique characteristics of mesoporous carbon.

From the viewpoint of metal−support interactions (MSI), the metal is basically more finely dispersed on the support surface due to stronger interactions.[31,32] It is evident that the chemical nature is different between the inside and the outside surfaces, but the occlusion of Pt into the carbon cell (Figure 9) cannot be explained by the strength of the MSI. It is more likely to be due to percolation of the solution into the carbon cells and retarded vaporization of the solvent during the dry-up process. Therefore, the large differences in the distributions of platinum can be attributed to the "wettability" of the solvent being different inside and outside of the carbon spheres. This effect usually causes the metal salts to become concentrated in certain parts of the porous materials and therefore leads to the formation of catalysts that lack uniform distribution of the metal. Our results for MCF carbon demonstrate that a confined space at the mesoscopic level can concentrate the metals during impregnation and may offer the possibility for the synthesis of novel materials.

Conclusion

Mesoporous cellular foam (MCF) carbon was successfully prepared by the reverse replication of MCF−silicas originally reported by Schimidt-Winkel et al. The two-step impregnation of sucrose followed by carbonization under flowing argon at 900 °C resulted in the formation of spherical hollow carbon with mesopores of ca. 4 nm. During temperature-programmed oxidation, the mesoporous carbon released argon above 600 °C, where oxidation of the carbon occurred. This result implies that micro- or mesopores running through the carbon walls are negligible and that the 4 nm pores are due to the interspheric spaces. The single-step impregnation of sucrose resulted in open-walled mesospheres with pore sizes of 4, 18, and 24 nm. The latter two pore sizes can be attributed to the window and the cell diameter, respectively, as in MCF−silica. Samples of platinum supported by these MCF carbons were prepared by the impregnation of a solution of $[Pt(NH_3)_4](NO_3)_2$. Platinum was highly dispersed (∼0.4 nm) on the closed mesospheric carbon, while it grew to particles of 15 nm in diameter in the pores of the open spheres, which agrees with the size of the carbon cells estimated by nitrogen adsorption and by SAXS.

Acknowledgment. A part of this study was financially supported by a Grant-in-Aid for Scientific Research on Priority Areas (Grant No. 13134101) from the Ministry of Education, Culture, Sports, Science and Technology.

Supporting Information Available: Additional experimental details and figures (PDF). This material is available free of charge via the Internet at http://pubs.acs.org.

CM0494296

(31) Haller, G. L.; Resasco, D. E. *Adv. Catal.* **1989**, *36*, 173.
(32) Tauster, S. J. *Strong Metal-Support Interactions*; Baker, R. T. K., Tauster S. J., Dumesic, J. A., Eds.; ACS Symposium Series 298; American Chemical Society: Washington, DC, 1986; Chapter 1.